Received: 7 December 2019 | Revised: 12 February 2020 | Accepted: 17 March 2020

DOI: 10.1002/app.49412

ARTICLE

Applied Polymer SCIENCE WILEY

Silane-functionalized Al_2O_3-modified polyurethane powder coatings: Nonisothermal degradation kinetics and mechanistic insights

Behzad Shirkavand Hadavand[1] | **Maryam Jouyandeh**[2,3] | **Seyed Mohamad Reza Paran**[4] | **Reza Khalili**[2,3] | **Henri Vahabi**[2,3] | **Hamed Fakharizadeh Bafghi**[1] | **Fouad Laoutid**[5] | **P. Poornima Vijayan**[6] | **Mohammad Reza Saeb**[1]

[1]Department of Resin and Additives, Institute for Color Science and Technology, Tehran, Iran

[2]Université de Lorraine, CentraleSupélec, LMOPS, F-57000, Metz, France

[3]Laboratoire Matériaux Optiques, Photoniques et Systèmes, CentraleSupélec, Université Paris-Saclay, Metz, France

[4]Advanced Materials Group, Iranian Color Society (ICS), Tehran, Iran

[5]Laboratory of Polymeric & Composite Materials, Materia Nova Research Center, Mons, Belgium

[6]Department of Chemistry, Sree Narayana College for Women, Kollam, Kerala, India

Correspondence
Behzad Shirkavand Hadavand, Department of Resin and Additives, Institute for Color Science and Technology, P.O. Box 16765-654, Tehran, Iran.
Email: shirkavand@icrc.ac.ir,
Henri Vahabi, Université de Lorraine, Metz, France.
Email: henri.vahabi@univ-lorraine.fr; and
Mohammad Reza Saeb, Department of Resin and Additives, Institute for Color Science and Technology, P.O. Box: 16765-654, Tehran, Iran.
Email: saeb-mr@icrc.ac.ir

Abstract

This work reports on nonisothermal degradation kinetics of polyurethane (PU)-based powder coatings containing 1, 3, and 5%wt% vinyltrimethoxysilane functionalized Al_2O_3 (V-Al_2O_3) nanoparticles. Thermogravimetric analysis of PU/V-Al_2O_3 powder coatings with different V-Al_2O_3 contents has been performed at different heating rates. Variation of activation energy (E_a) of PU/V-Al_2O_3 powder coatings was modeled as a function of partial mass loss by using Kissinger–Akahira–Sunose, Ozawa–Wall–Flynn and modified Coats–Redfern isoconversional approaches. The results revealed hindered decomposition process of PU/V-Al_2O_3 nanocomposite powder coatings, featured by an increase in activation energy of degradation from ~158 for blank PU to 225, 183, and 229 kJ/mol for nanocomposites filled with 1, 3, and 5 wt% of V-Al_2O_3, respectively. Likewise, pre-exponential factor values increased for samples containing V-Al_2O_3 nanoparticles compared to that of blank sample. Sestak–Berggren kinetic model appropriately captured thermal degradation behavior of PU/V-Al_2O_3 nanocomposites than that of *n*th order decomposition kinetic reaction models.

KEYWORDS

crosslinking, differential scanning calorimetry, resins, theory and modeling, thermosets

1 | INTRODUCTION

The success of thermosetting powder coatings in the paint and varnish industry[1,2] roots in easy handling and applying, low-cost, energy savings, and acceptable performance features.[3] This kind of coating has revealed promising growth as industrial finishers thanks to little or no solvent required in material development.[4–6] Powder-

coated finishes have been widely used in different colors for interior and exterior applications such as automotive, domestic appliances, architectural elements, agricultural machines, sterilization equipment, food, and medical industries.[7] Extensive use of powder coatings was due to their high resistant to scratch and abrasion, anticorrosion properties, and survival in chemical environment.[8]

Thanks to the multitude of soft and hard blocks and versatile properties, polyurethanes (PUs) have been increasingly considered as coatings.[9,10] On the other hand, toxicity of first-generation PU coatings turned attention toward biodegradable and environmentally friendly PU coatings. For example, a green route was introduced for synthesizing non-isocyanate PU via reaction between monomers of di-functional and poly-functional cyclic carbonate and di-functional and poly-functional primary alkyl amines.[11,12] Pilch-Pitera[13,14] synthesized biodegradable PU crosslinker using alicyclic diisocyanates and monohydric aliphatic alcohols as well as dibutyltin dilaurate and triethylamine. However, in the form of powder coating, PU could give favorable properties like excellent resistance against chemicals and moisture, high stiffness, and acceptable anticorrosion properties because of its high degree of crosslinking.[15,16] PU powder coatings are not normally stable in harsh circumstances, for example, high stress, thermal shock, direct exposure to UV light, and heat. The cracking of PU coatings is quite often the consequence of thermal degradation of polymer chains.[17] Thermal degradation subsequently makes the service lifetime shorten.[9] Moreover, high flammability and production of large amount of smoke and toxic gases are known as further weaknesses of PU powder coatings.[18]

With the progress of technology, nano-sized solid particles including high innate thermally stable materials such as metal oxides,[19,20] carbon-based nanoparticles,[21] silica,[22,23] clays,[24–28] and ceramic[29] dispersed in a host polymer have opened promising gates toward high-performance coatings. Among metal oxide nanoparticles, nano-Al_2O_3 considered an efficient modifier for the polymers, for example, to enhance anticorrosion properties of coatings,[30,31] hydrophobicity,[32] scratch, and abrasive resistance.[30,33] Organic modification of metal oxides has also been recognized for strengthening the interfacial interaction between the metal oxide and polymers. For instance, toluene-2,4-diisocyanate modified nano-Al_2O_3 was used to enhance wear resistance of phenolic coatings.[34] In another report, vinyltrimethoxysilane (VTMS)-modified aluminum oxide (Al_2O_3) took credit for its ability to improve mechanical strength, chemical and thermal stability, scratch, and abrasion resistance of the neat polymer coating.[35] It was also reported that appropriate dispersion of Al_2O_3 nanoparticles improves the thermal properties of PU coatings.[36,37]

Mechanistic description of thermal decomposition/degradation kinetics of PU nanocomposite powder coatings assists in optimum formulation and processing conditions for obtaining thermally stable coatings.[38] Nanoparticles can play the role of barrier protecting agents to prevent polymer chains from thermal decomposition via formation of a char layer on the top of the coatings.[39–42] Extensive research addressed enhancement of thermal stability of polymers by the addition of nanoparticles.[43,44] In contrast, a few reports have mentioned thermal decomposition kinetics of coatings by modeling of activation energy of degradation process based on thermogravimetric analysis (TGA) data.[45] Thermal degradation changes the chemical structure and physical properties of polymeric coatings. In the case of polymeric powder coatings, thermal degradation mechanism is an inherently complex phenomenon. Degradation involves molecular scission and subsequently results in variation of molecular weight distribution in the material. The complexity of thermal degradation mechanism of a powder coating increases dramatically in the presence of nanoparticles, for a multistep phenomenon may occur. Study of degradation kinetics of powder coatings nanocomposites by computational methods provides insights for mechanistic explanation of degradation, but for PU powder coatings no report has been found by the authors of this work. In this work, the effect of the amount of VTMS-functionalized Al_2O_3 nanoparticles (V-Al_2O_3) on the thermal stability of PU powder coating was investigated using TGA experimental data. Surface functionalization of Al_2O_3 with VTMS was studied by Fourier transform infrared (FT-IR) technique, while the state of dispersion of nanoparticles in the PU matrix was observed by scanning electron microscopy (SEM). Nonisothermal kinetics of degradation of PU/Al_2O_3 nanocomposites was modeled by the integral isoconversional methods including Flynn–Wall–Ozawa (FWO), Kissinger–Akahira–Sunose (KAS), and the modified Coats–Redfern (m-CR). The activation energy of decomposition reaction was calculated as a function of partial mass loss. Eventually, the models were checked by experimental results.

2 | EXPERIMENTAL

2.1 | Materials

PU powder coating resin (9016 WU18AX) was formulated with PU resin, technical grade of benzoin degassing agent (Anadolu Kimya Company, Turkey), Vestagon B 1530 as a curing agent (Evonik Resource Efficiency GmbH, Germany) by Peka Chimie Company (Iran) and used as a polymer matrix. Nano-Al_2O_3 with particle size

around 40 nm was produced by US Research Nanomaterials Inc. Modification of nanoparticles was carried out by VTMS coupling agent and isopropyl alcohol solvent purchased from Merck Company (Germany). All the materials were used as received.

2.2 | Sample preparation

First, nano-Al_2O_3 particles were chemically modified with VTMSin isopropyl alcohol.[7,35] Silane modification of Al_2O_3 nanoparticles is schematically shown in Figure 1.[46] Then, PU powder coating resin, TiO_2, benzoin, baric, and varying amount (1, 3, and 5 wt%) of modified nano-Al_2O_3 particles were extruded in the twin-screw extruder (Yantai Donghui Powder Processing Equipment Company, China) for preparing different chips of nanocomposites (Table 1).

These chips were powdered by milling and sieved such that roughly 70% of particles reached an average particle size of 55 μm with some having more or less sizes. The resulting powder nanocomposites were coated on 10 × 15 cm metal plates by electrostatic method and cured at 180°C for 15 min.

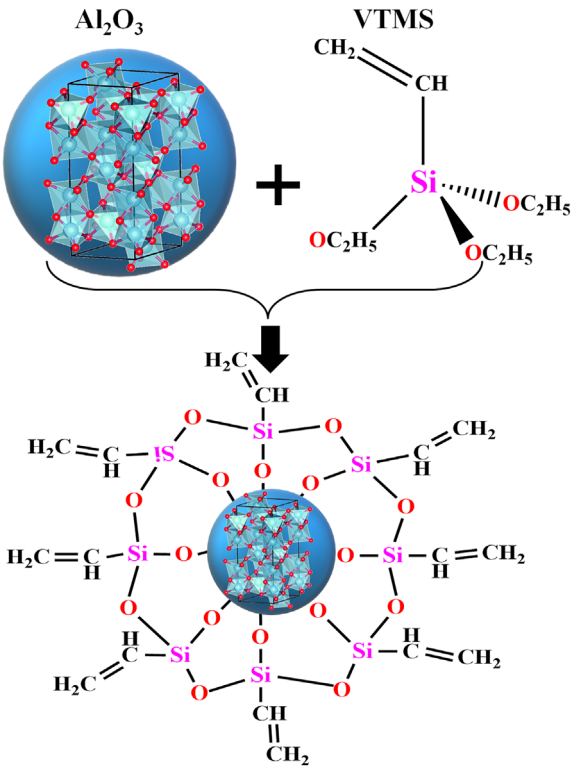

FIGURE 1 The structure of VTMS-functionalized Al_2O_3 nanoparticles [Color figure can be viewed at wileyonlinelibrary.com]

TABLE 1 Weight composition of polyurethane (PU) nanocomposite powder coatings

Item	Sample code	V-Al_2O_3 content (wt%)
1	PU	0
2	PU/V-Al_2O_3-1	1
3	PU/V-Al_2O_3-3	3
4	PU/V-Al_2O_3-5	5

Abbreviation: PU, polyurethane.

2.3 | Characterization

2.3.1 | Fourier transform infrared spectroscopy

Al_2O_3 nanoparticles surface modified with VTMS was characterized on a FT-IR instrument of Spectrum one, PerkinElmer Inc. (Boston, MA). Al_2O_3 and modifiedAl_2O_3 powders were formed as pellet by the aid of KBr to collect FT-IR spectra in a transmission mode within the wavelength range of 4,000 to 400 cm^{-1} at 4 cm^{-1} resolutions.

2.3.2 | SEM analysis

The dispersion state of VTMS-modified Al_2O_3 nanoparticles in PU polymer matrix was studied using SEM. The micrographs were provided from the fractured surface of prepared PU nanocomposite powder coatings by Hitachi S-4160 SEM.

2.3.3 | Thermal decomposition characterization

TGA analysis for each nanocomposite sample was conducted by Setaram Labsys Evo thermogravimetric analyzer (France). Prior to testing, all the samples were dried at 60°C for 12 hr for removal of their moisture. TGA measurement was performed under nitrogen atmosphere with fixed gas flow rate of 100 cm^3/min in the temperature range of 25–800°C with various heating rates of 5, 10, 15, and 20°C/min for each sample.

3 | RESULTS AND DISCUSSION

FT-IR spectra of Al_2O_3 and VTMS-modified Al_2O_3 nanoparticles are shown in Figure 2. Al—O bonds of Al_2O_3 structure can be observed at characteristic peaks of at 587, 751, and 809 cm^{-1}. The band at 3,449 cm^{-1} is attributed to O—H stretching and O—H bending vibration

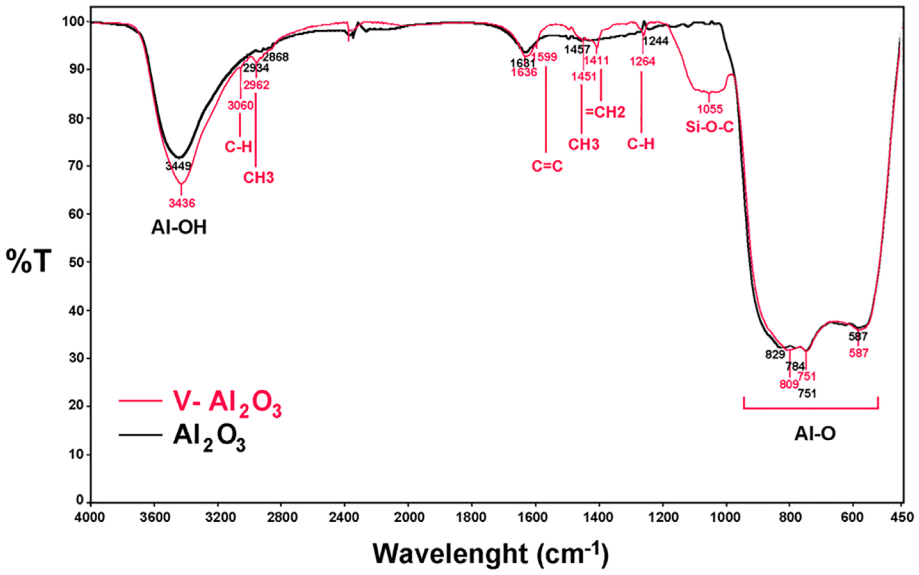

FIGURE 2 FT-IR spectra of nano-Al_2O_3 and nano-V-Al_2O_3 [Color figure can be viewed at wileyonlinelibrary.com]

is visible at 1,631 cm^{-1}. In the FT-IR spectrum of VTMS-modified Al_2O_3 the peaks at 3,060 cm^{-1} is attributed to C—H stretching in —CH═CH_2, 2,962 cm^{-1} is for CH_3 stretching in OCH_3, 1,599 cm^{-1} is related to C═C stretching in CH═CH_2, 1,451 cm^{-1} shows CH_3 asymmetric deformation in OCH_3, 1,411 cm^{-1} is attributed to ═CH_2 in-plan deformations in CH═CH_2, 1,264 cm^{-1} shows C—H in-plan deformations in CH═CH_2 and asymmetric stretch Si—O—C is visible at 1,055 cm^{-1}. SEM micrographs of the neat PU and dispersion fashion of samples containing 1, 3, and 5 wt% V-Al_2O_3 nanoparticles were provided from the fracture surface of the PU/V-Al_2O_3 powder coatings (Figure 3). By comparing SEM micrographs of PU/V-Al_2O_3 powder nanocomposite coatings with that of neat PU coating, it appears that V-Al_2O_3 nanoparticles are distributed almost homogeneously in the PU matrix. This is because the C═C bond on the surface of V-Al_2O_3 can participate in curing process of PU via radical polymerization leading to a relatively uniform dispersion.[29,30] However, as marked in Figure 3, some agglomeration can also be observed in the PU resin. It is also evident from SEM images that aggregations became larger by increasing V-Al_2O_3 nanoparticles loading. Thermal degradation of PU/V-Al_2O_3 nanocomposites at different compositions of 1, 3, and 5 wt% was examined based on TGA experimental data to postulate the contribution of this nanoparticle to the thermal stability of PU powder coatings. Figure 4 shows TGA thermograms of the cured blank PU and its nanocomposite films containing 1, 3, and 5 wt% of V-Al_2O_3 nanoparticles. DTG curves giving some clue about the mass loss variation from the composites while heating during the degradation process[47] are also shown in Figure 5. A slight drop around 110°C can be observed for all the samples, which is related to evaporation of absorbed water and moisture, solvent, and unreacted materials. The main weight loss of the samples occurred between 300 and 400°C due to the decomposition of the polymer chains. The complete decomposition of PU happened around 500°C. Thermal decomposition fingerprint of the PU nanocomposites containing different V-Al_2O_3 loadings were taken by using common degradation temperatures, including the temperature at which 5% weight loss (T_5), the temperature at which 10% weight loss (T_{10}) signifying early-stage footprints of degradation, and also the temperature at which maximum weight loss (T_p) occurs, are extracted from the TGA diagrams at low and high heating rates of 5 and 20°C/min (Table 2). Overall, higher values of T_5 observed for nanocomposite containing 1, 3, and 5 wt% of Al_2O_3 nanoparticles is indicative of significant enhancement of thermal stability at early stage of decomposition comparison with PU. According to statistics, the value of T_5 at low heating rate of 5°C/min was increased from 228.1°C for PU to 268.7°C (~19.3%), 271.9°C (~18%), and 260.4°C (~14%) for PU/V-Al_2O_3-1, PU/V-Al_2O_3-3, and PU/V-Al_2O_3-5 samples, respectively. Likewise, there was a rise in T_{10} value from 305.5°C for PU to 327.5°C (~7.2%), 325.8°C (~6.6%), and 325.4°C (~6.5%) for PU/V-Al_2O_3-1, PU/V-Al_2O_3-3, and PU/V-Al_2O_3-5, respectively. From Figure 4 and Table 2, it can be concluded that the addition of 3 wt% of V-Al_2O_3 nanoparticles to PU matrix can feelingly improve thermal stability and char forming of PU compared to samples with 1 and 5 wt% of V-Al_2O_3 nanoparticles. The enhancement of thermal stability of PU nanocomposites at early decomposition period can be ascribed to the physical prevention effect of the V-Al_2O_3 nanoparticles that prevent the escape of volatile compounds and free radicals

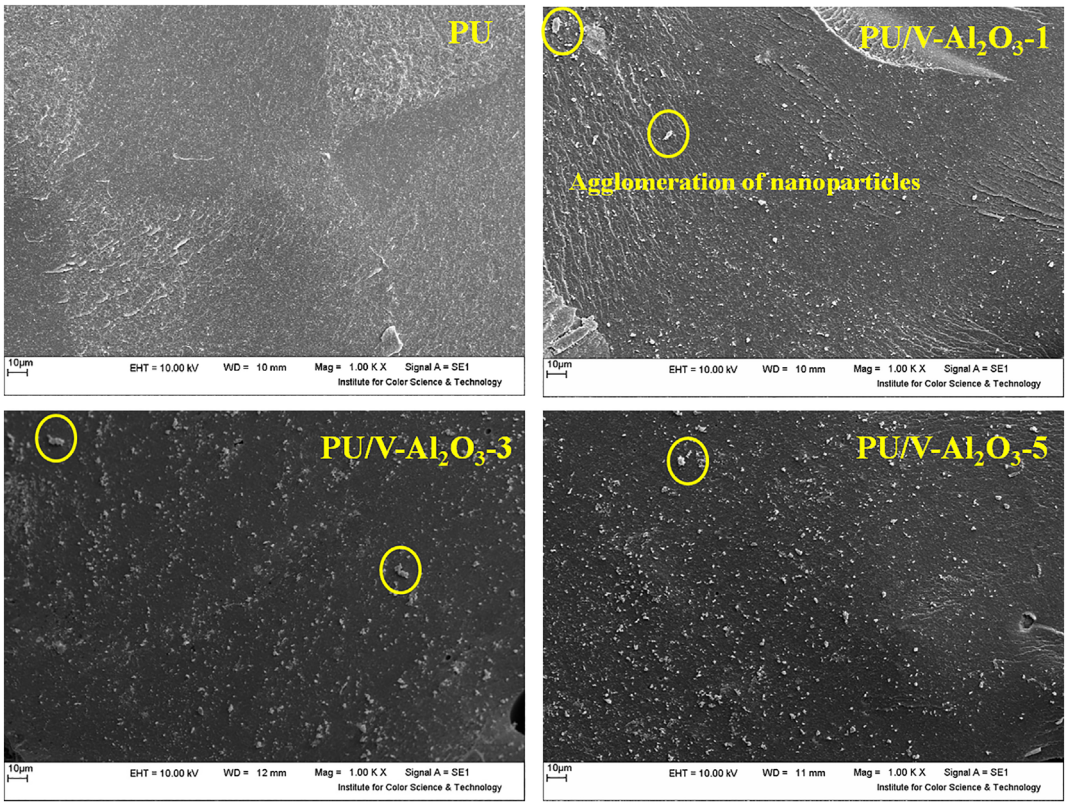

FIGURE 3 SEM micrographs of neat PU and its nanocomposites containing 1, 3, and 5 wt% of V-Al_2O_3 [Color figure can be viewed at wileyonlinelibrary.com]

produced through polymer chain scission. In fact, silane-coupling agents attached to the surface of Al_2O_3 nanoparticles can improve the dispersion stability of V-Al_2O_3 nanoparticles throughout PU matrix. Moreover, VTMS can enhance the compatibility of inorganic nanoparticles with organic matrix.[48] This can improve interfacial interaction between nanoparticles and PU matrix that restrict the movement of polymer chains in the vicinity of nanoparticles.[49] The V-Al_2O_3 nanoparticles can interact with PU matrix through the Van der Waals interaction and hydrogen bonding. Schematic of typical interaction and dispersion state of V-Al_2O_3 nanoparticles in the PU matrix is shown in Figure 6. A small fall in T_5 and T_{10} of PU/V-Al_2O_3-5 compared to PU/V-Al_2O_3-1 and PU/V-Al_2O_3-3 nanocomposites is probably due to the partial agglomeration of V-Al_2O_3 nanoparticles at 5 wt%, which leads to formation of free volume in the nanocomposite network assisting in easier movement of molecules in the vicinity of the nanoparticles.[50] According to Table 2, the rise in residue values can be observed upon increasing V-Al_2O_3 nanoparticles content in the system due to very high thermal stability of V-Al_2O_3 nanoparticles up to 830°C. The degree of the degradation or the partial mass loss (α) is defined as[51]:

$$\alpha = \frac{(W_0 - W_t)}{(W_0 - W_f)} \quad (1)$$

where W_0 is the initial weight of polymer, W_t is the weight of polymer at time t, and W_f is the weight of polymer at the end of degradation reaction. The $\alpha - T$ profiles at different heating rates for blank PU, PU/V-Al_2O_3-1, PU/V-Al_2O_3-3, and PU/V-Al_2O_3-5 are compared in Figure 7. It was found that the degradation step ($\alpha - T$) varies with heating rates. At lower heating rates, when the pyrolysis progress slows down, the onset and endset degradation temperatures were both low. In contrast, the onset and endset degradation temperatures were shifted to the elevated temperatures at higher heating rates when the pyrolysis became fast. The thermal decomposition rate of polymer system is measured by the following equation[52]

$$\frac{d\alpha}{dt} = k(T)f(\alpha) \quad (2)$$

In Equation (2), $f(\alpha)$ is the reaction model and $k(T)$ is the reaction rate constant, which is defined based on Arrhenius equation as[53]:

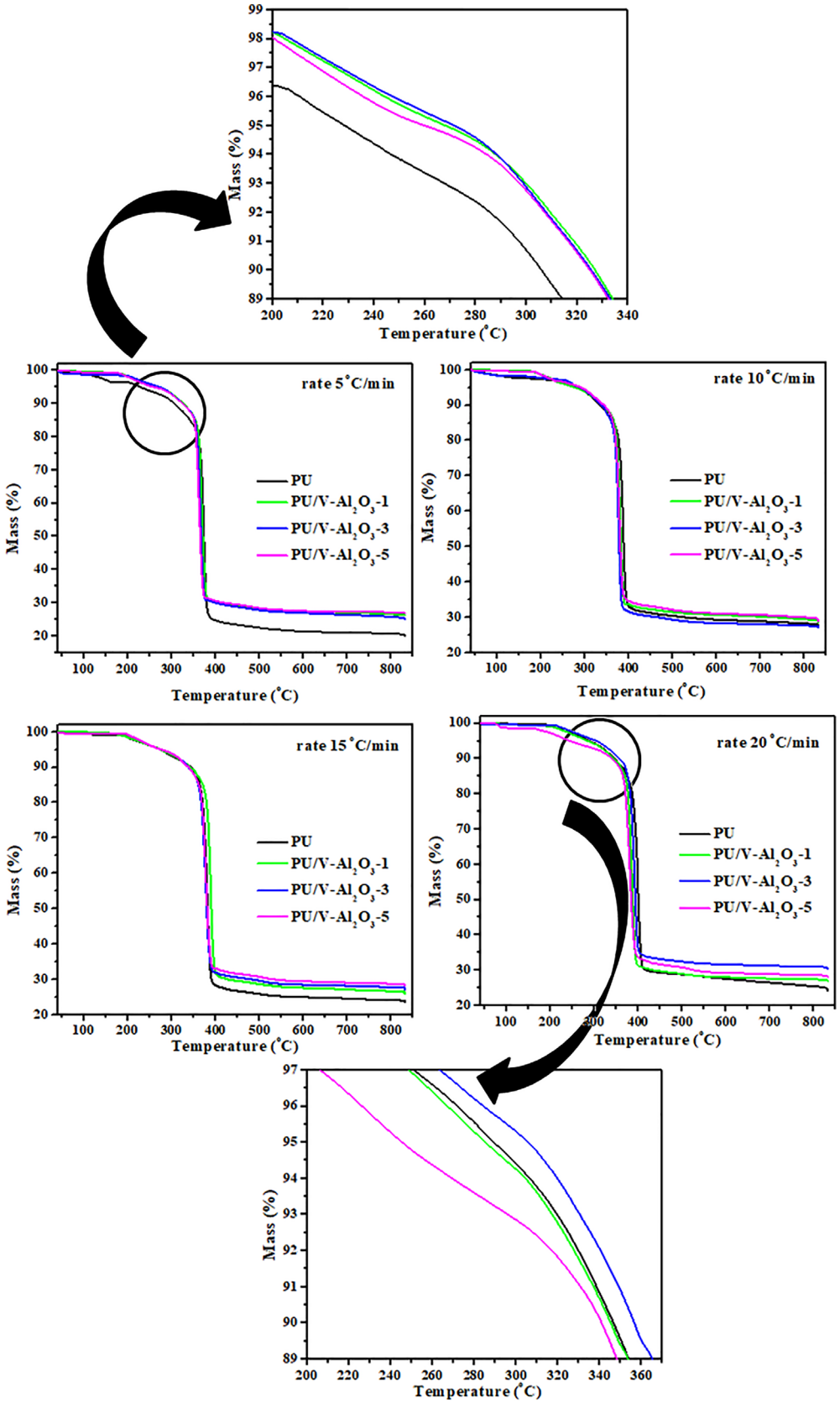

FIGURE 4 TGA thermograms of PU/V-Al_2O_3 nanocomposites at different heating rates [Color figure can be viewed at wileyonlinelibrary.com]

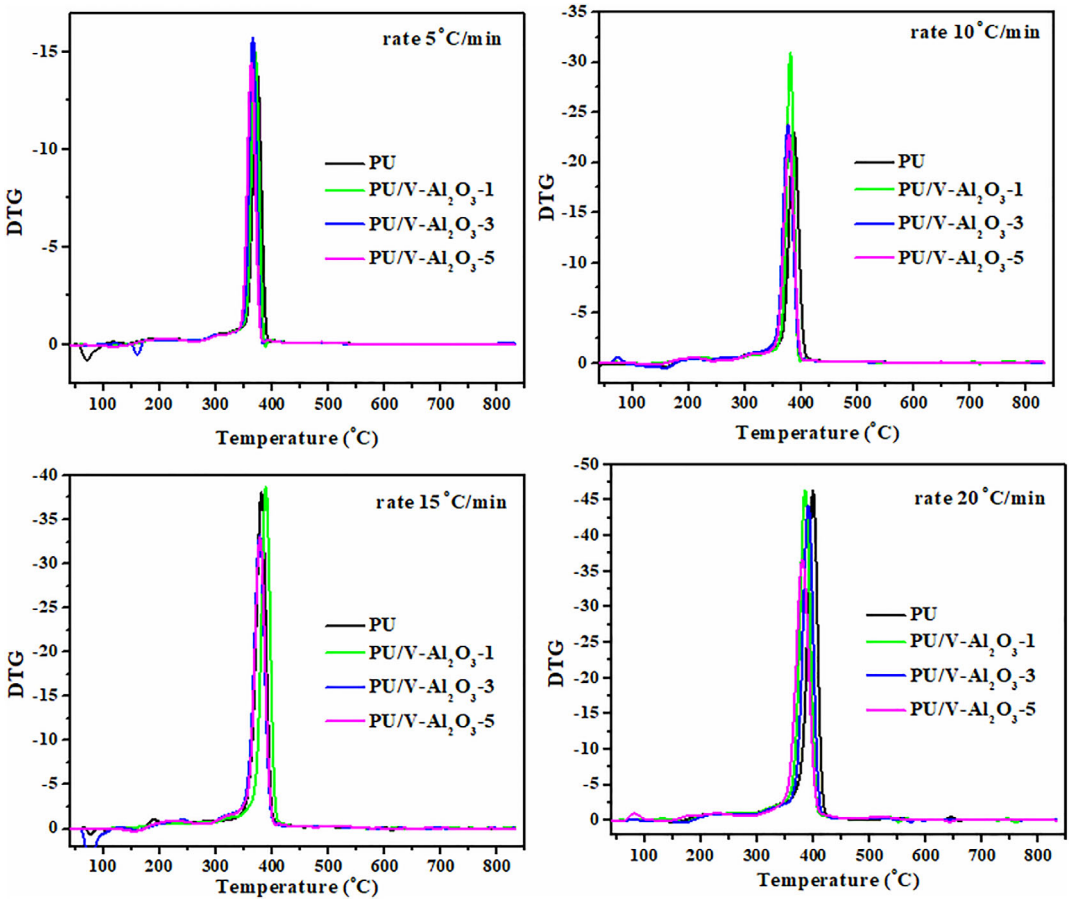

FIGURE 5 DTG thermograms of PU/V-Al_2O_3 nanocomposites at different heating rates [Color figure can be viewed at wileyonlinelibrary.com]

TABLE 2 Thermal decomposition characteristics of PU/Al_2O_3 nanocomposites derived from TGA diagrams at low-heating rate of 5°C/min and at high-heating rate of 20°C/min

Designation	T_5 (°C)	T_{10} (°C)	T_P (°C)	Residue (%)	T_5 (°C)	T_{10} (°C)	T_P (°C)	Residue (%)
Heating rate	–	5°C/min	–	–	–	20°C/min	–	–
Neat PU	228.3	305.5	372.9	19.9	288.9	346.5	399.6	24.2
PU/V-Al_2O_3-1	268.7	327.5	369.7	24.9	285.3	344.9	384.9	27.0
PU/V-Al_2O_3-3	271.9	325.8	365.6	26.1	305.3	356.3	390.6	30.3
PU/V-Al_2O_3-5	260.4	325.4	362.7	26.9	245.1	340.7	380.4	28.1

Abbreviations: Al_2O_3, aluminum oxide; PU, polyurethane; TGA, thermogravimetric analysis.

$$k(T) = A\exp\left(-\frac{E_a}{RT}\right) \quad (3)$$

where A is the pre-exponential factor, R is the universal gas constant, and E_α is the activation energy of the thermal decomposition reaction.

The model-free isoconversional approach is used to study polymer decomposition mechanism due to its complexity, which prevents the use of a single equation across the whole temperature range.[54–57] By considering the model-free isoconversional method, the thermal decomposition rate is assumed to be only function of temperature at a constant degree of degradation.

The model-free isoconversional method is divided into two types of differential and integral methods. However, applying differential method to integral data (e.g., TGA) requires numerical differentiation. Numerical differentiation brings noise in the data and smoothing the same also brings inaccuracy, which ultimately leads to the discontinuous activation energy profile and erratic

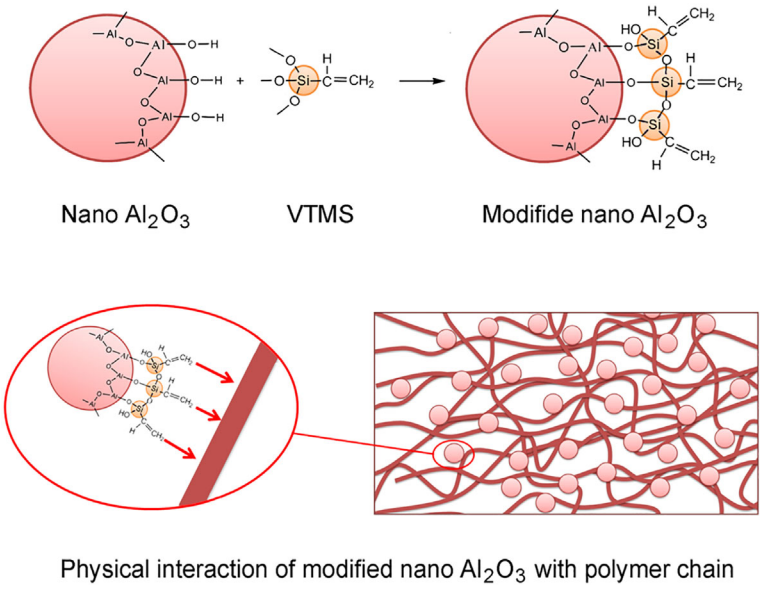

FIGURE 6 Schematic of typical interaction and dispersion state of V-Al_2O_3 nanoparticles in PU matrix [Color figure can be viewed at wileyonlinelibrary.com]

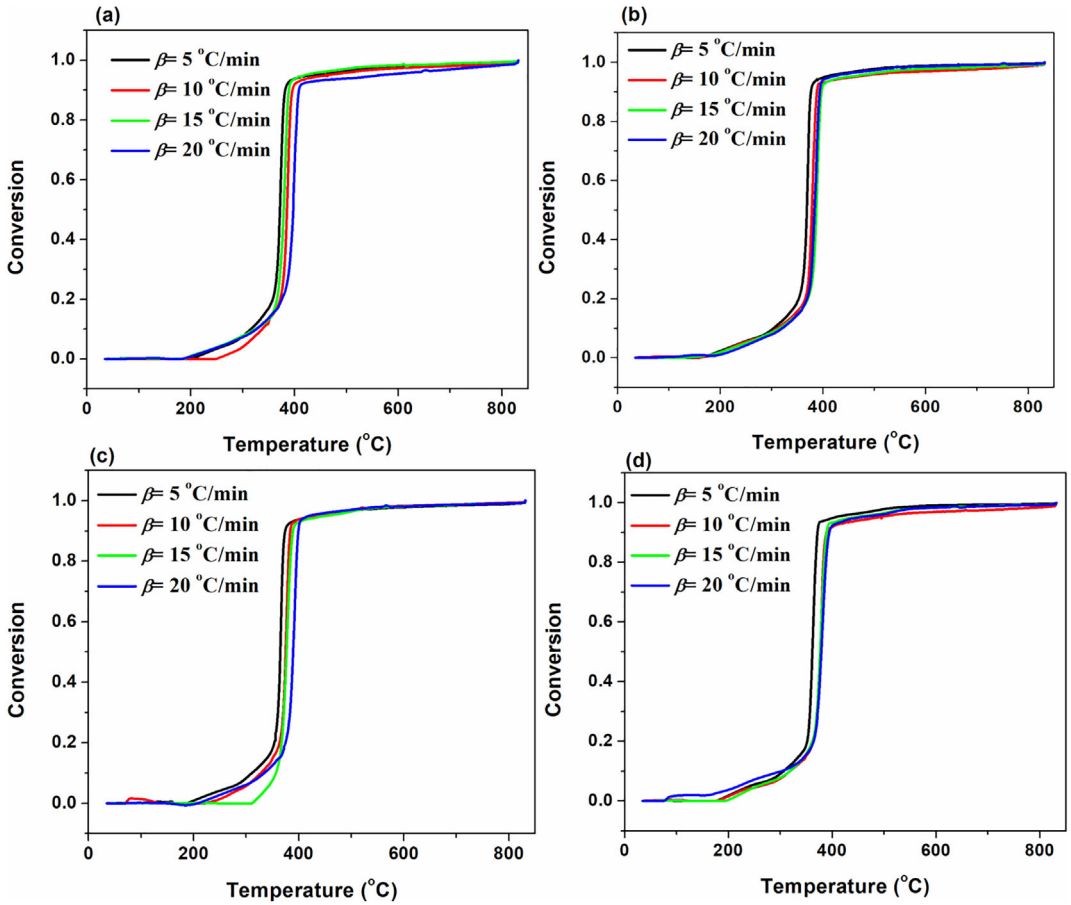

FIGURE 7 Degradation conversion profiles at various heating rates for (a) blank PU, (b) PU/V-Al_2O_3-1, and (c) PU/V-Al_2O_3-3 [Color figure can be viewed at wileyonlinelibrary.com]

trend.[58] Therefore, integral isoconversional methods are prioritized.

FWO is one of the most frequently used integral isoconversional method which leads to calculation of E_α through the slope of the diagram of $\ln(\beta_i)$ versus $1/T_\alpha$ at certain α that is defined as follows[59]:

$$\ln(\beta_i) = \text{Const} - 1.052\left(\frac{E_\alpha}{RT_\alpha}\right) \quad (4)$$

The *KAS* is an well-known and more accurate integral isoconversional method which can predicts the activation energy of the degradation reaction by the slope of the curve of $\ln\left(\frac{\beta_i}{T^2_{\alpha,i}}\right)$ versus $1/T$ through the following equation[60]:

$$\ln\left(\frac{\beta_i}{T^2_{\alpha,i}}\right) = \text{Const} - \left(\frac{E_\alpha}{RT_\alpha}\right) \quad (5)$$

The multi-heating rate application of the CR method,[61] which named *m-CR*,[62] is used as another isoconversional method and defined as[63]:

$$\ln\left[\frac{\beta}{T^2(1-2RT/E_\alpha)}\right] = \ln\left[\frac{-AR}{E_\alpha \ln(1-\alpha)}\right] - \frac{E_\alpha}{RT}. \quad (6)$$

According to Equation (6), plotting $\ln\left[\frac{\beta}{T^2(1-2RT/E_\alpha)}\right]$ at a constant conversion of each heating rate against $1/T$ leads to a family of straight lines whose slopes give the activation energies of degradation reaction and then E_α values are substituted into the intercept to obtain frequency factor (A). As both sides of m-CR method are functions of activation energy, the calculation is done iteratively by considering a value for E_α as first assumption. The recalculation process continues until convergence occurs. The E_α values that obtained from KAS and

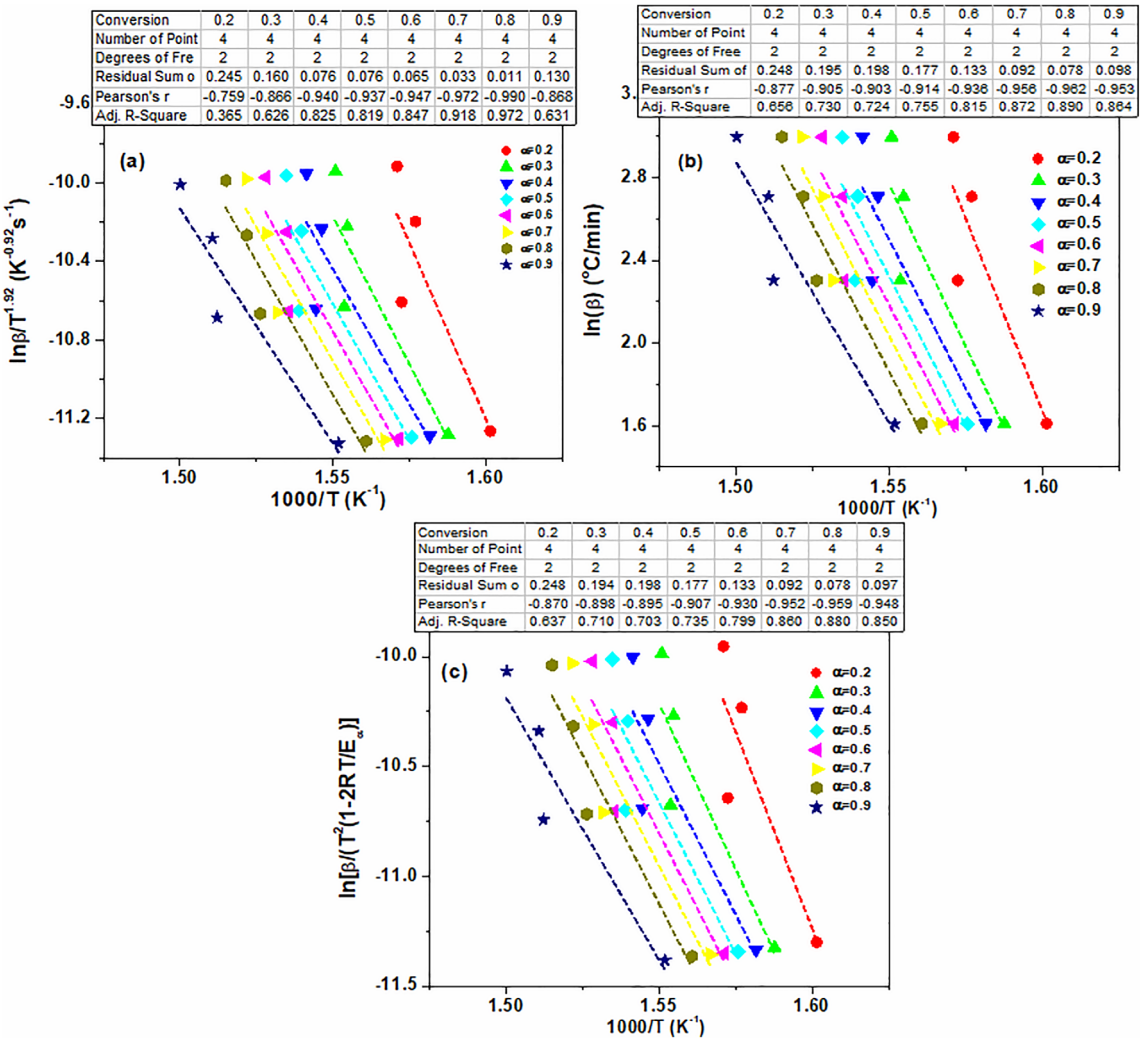

FIGURE 8 Typical isoconversional plots for PU/ V-Al_2O_3nanocomposites (a) KAS, (b) FWO, and (c) m-CR methods [Color figure can be viewed at wileyonlinelibrary.com]

FWO methods can be used as a first guess for iterative method to reach the complete solution of Equation (6).

Figure 8 shows the isoconversional plots PU/V-Al_2O_3 nanocomposites. It is clear from Figure 8 that the fitted lines in the for KAS, FWO, and m-CR methods are almost parallel with each other especially at $0.3 \leq \alpha \leq 0.8$, which indicates that a single mechanism exists for thermal decomposition kinetics of PU/V-Al_2O_3 nanocomposites.[64] Figure 9 reveals variation of activation energy of thermal decomposition reaction with respect to degree of conversion for blank PU, PU/V-Al_2O_3-1, PU/V-Al_2O_3-3, and PU/V-Al_2O_3-5 nanocomposites based on three isoconversional methods. From Figure 9, it is clear that all the isoconversional methods of KAS, FWO, and m-CR yielded similar values of activation energy. As the decomposition rate is low under the α values of 0.2 and above 0.9 the equipment sensitivity probably lead to the data aberrations.[52] Therefore, the conversion regime in these ranges have been removed. By proceeding of thermal decomposition process PU systems, the activation energy remained nearly unchanged or shows only a slight change after the initial stage of decomposition between the conversion range of α = 0.3–0.8 for all the samples. A slight drop in activation energies before α = 0.3 indicate that the degradation reaction starts easily due to the existence of thermally unstable bonds and weak links which explains the lower values of activation energy at the beginning of the decomposition process.[45,65] Moreover, it was found that the addition of V-Al_2O_3 nanoparticles into PU matrix effectively retarded the thermal decomposition of system. By substituting Equation (3) in Equation (2), the rate of the thermal decomposition can be obtained as:

$$\frac{d\alpha}{dt} = A\exp\left(-\frac{E_a}{RT}\right)f(\alpha) \tag{7}$$

The goal of empirical kinetics is to find an $f(\alpha)$ function fulfilling the mathematical requirements of Equation (7). Besides the kinetic models derived from the geometry of a reacting interface, there are also formal expressions of the $f(\alpha)$ function which correlate as close as possible with the experimental data. The nth order decomposition reaction is as follows[66]:

$$f(\alpha) = (1-\alpha)^n \tag{8}$$

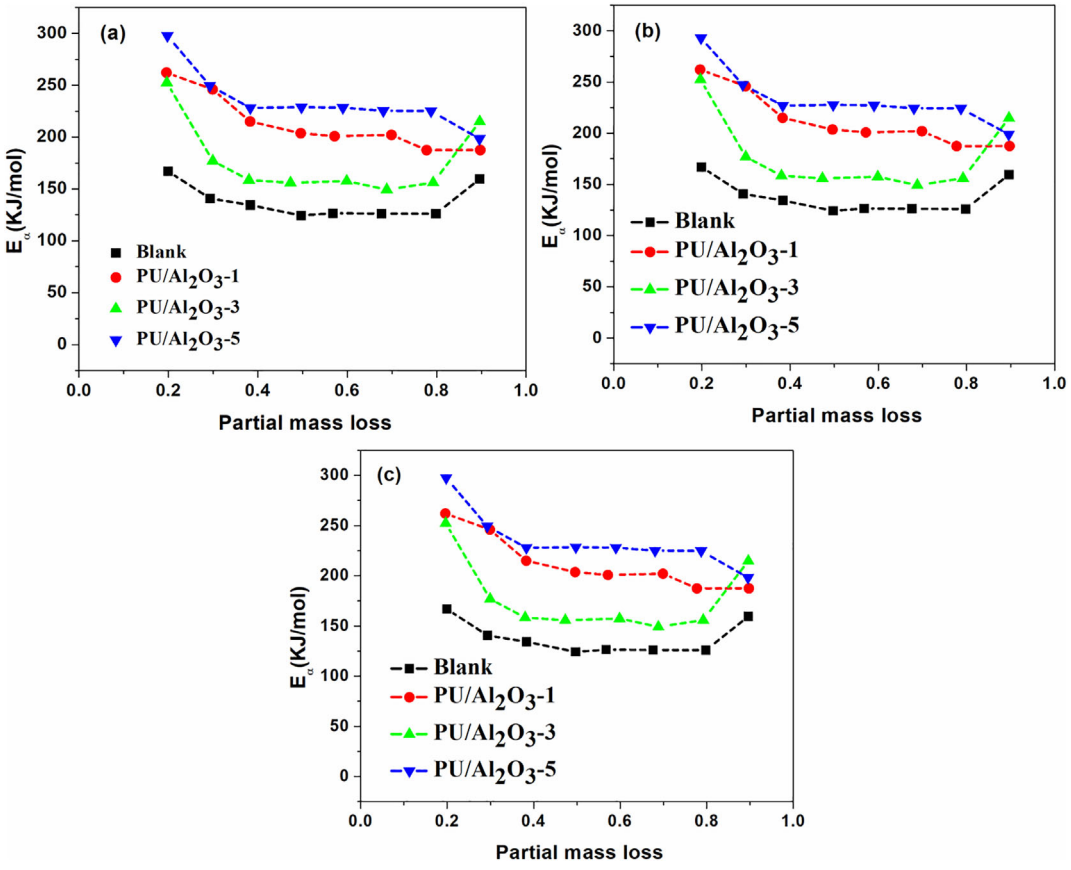

FIGURE 9 Activation energy of blank PU and its nanocomposites containing 1, 3, and 5 wt% of V-Al_2O_3 nanoparticles in terms of partial mass loss obtained using (a) KAS, (b) FWO, and (c) m-CR methods [Color figure can be viewed at wileyonlinelibrary.com]

TABLE 3 Decomposition parameters based on the *n*th order decomposition reaction of PU and PU nanocomposites calculated using different isoconversional kinetic models

	KAS			FWO			m-CR		
Designation	E_α (kJ/mol)	ln (A) (min^{-1})	n	E_α (kJ/mol)	ln (A) (min^{-1})	n	E_α (kJ/mol)	ln (A) (min^{-1})	n
Blank	158.03	20.99	2.33	160.54	23.7	2	157.62	24.2	1.96
PU/Al_2O_3-1	225.59	41.41	0.87	224.65	41.54	0.85	225.32	41.36	0.87
PU/Al_2O_3-3	183.42	28.7	1.83	184.52	29.29	1.78	183.07	29.53	1.76
PU/Al_2O_3-5	228.57	28.21	1.46	227.36	34.17	0.96	229.19	34.13	0.96

Abbreviations: Al_2O_3, aluminum oxide; FEO, Ozawa–Wall–Flynn; KAS, Kissinger–Akahira–Sunose; m-CR, modified Coats–Redfern; PU, polyurethane.

TABLE 4 Decomposition parameters based on the Sestak and Berggren decomposition reaction of PU nanocomposites calculated using different isoconversional kinetic models

	KAS				FWO				m-CR			
Designation	E_α (kJ/mol)	ln (A) (min^{-1})	m	n	E_α (kJ/mol)	ln (A) (min^{-1})	m	n	E_α (kJ/mol)	ln (A) (min^{-1})	m	n
Blank	158.03	30.42	1.92	1.48	160.54	30.87	1.90	1.47	157.62	30.35	1.92	1.49
PU/Al_2O_3-1	225.59	42.08	0.99	0.76	224.65	41.92	1.00	0.77	225.32	42.04	1.00	0.76
PU/Al_2O_3-3	183.42	35.42	1.65	1.32	184.52	35.63	1.65	1.31	183.07	35.36	1.65	1.32
PU/Al_2O_3-5	228.57	43.69	1.28	1.33	227.36	43.48	1.29	1.33	229.19	43.69	1.29	1.32

Abbreviations: Al_2O_3, aluminum oxide; FEO, Ozawa–Wall–Flynn; KAS, Kissinger–Akahira–Sunose; m-CR, modified Coats–Redfern; PU, polyurethane.

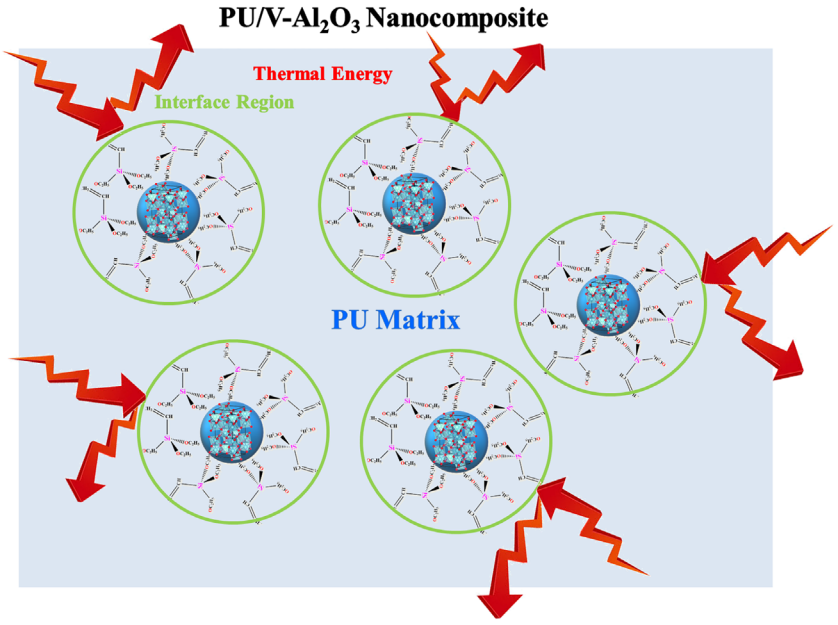

FIGURE 10 Mechanistic explanation of restriction of thermal energy in the coating matrix due to the presence of strong PU/(V-Al_2O_3) interface [Color figure can be viewed at wileyonlinelibrary.com]

Moreover, Sestak and Berggren[67] proposed an empirical kinetic model as follows:

$$f(\alpha) = \alpha^{m}(1-\alpha)^{n} \quad (9)$$

where m and n are reaction order and $(m + n)$ gives the overall order. Two kinetic exponents kinetic equation would provide a general expression for all the kinetic equations used for mathematical modeling of solid-state reactions. The average values of activation energy E_{α}, pre-exponential factor ln(A), and decomposition reaction order n of the nth order decomposition reaction for blank PU and its nanocomposites were obtained from Equation (8) and listed in Table 3. Moreover, the obtained values from Sestak and Berggren kinetic model Equation (9) is listed in Table 4.

The decomposition reaction order n and m in both kinetic models decreases by the addition of V-Al_2O_3 nanoparticles into PU matrix, which indicated that the rate of decomposition reaction decrease by introduction of nanoparticles. Introduction of highly stable V-Al_2O_3 nanoparticles make thermal decomposition reaction harder and slower due to the PU denser network as a result of strong chemical interactions of V-Al_2O_3 nanoparticles with PU matrix. High interfacial surface area in the vicinity of V-Al_2O_3 nanoparticles and PU matrix hardened the molecular motion and decrease the decomposition rate. The passage of heat is strictly restricted into strong matrix–filler interface region. This slows down the diffusion of heat through the epoxy matrix, which subsequently prevents extensive polymer chain session. Figure 10 represents the restriction of thermal energy by the interfacial region between PU and V-Al2O3 nanoparticles. Moreover, pre-exponential factor or the frequency factor ln(A) gives very useful information about the rate of vibration of the decomposition products which directly proportional to the E_{α}.[68] A rise in the frequency factor can be observed by introduction of V-Al_2O_3 nanoparticles in PU matrix which indicate that the presence of abundant V-Al_2O_3 nanoparticles led that polymer chains dissipate more energy and resist against thermal decomposition which

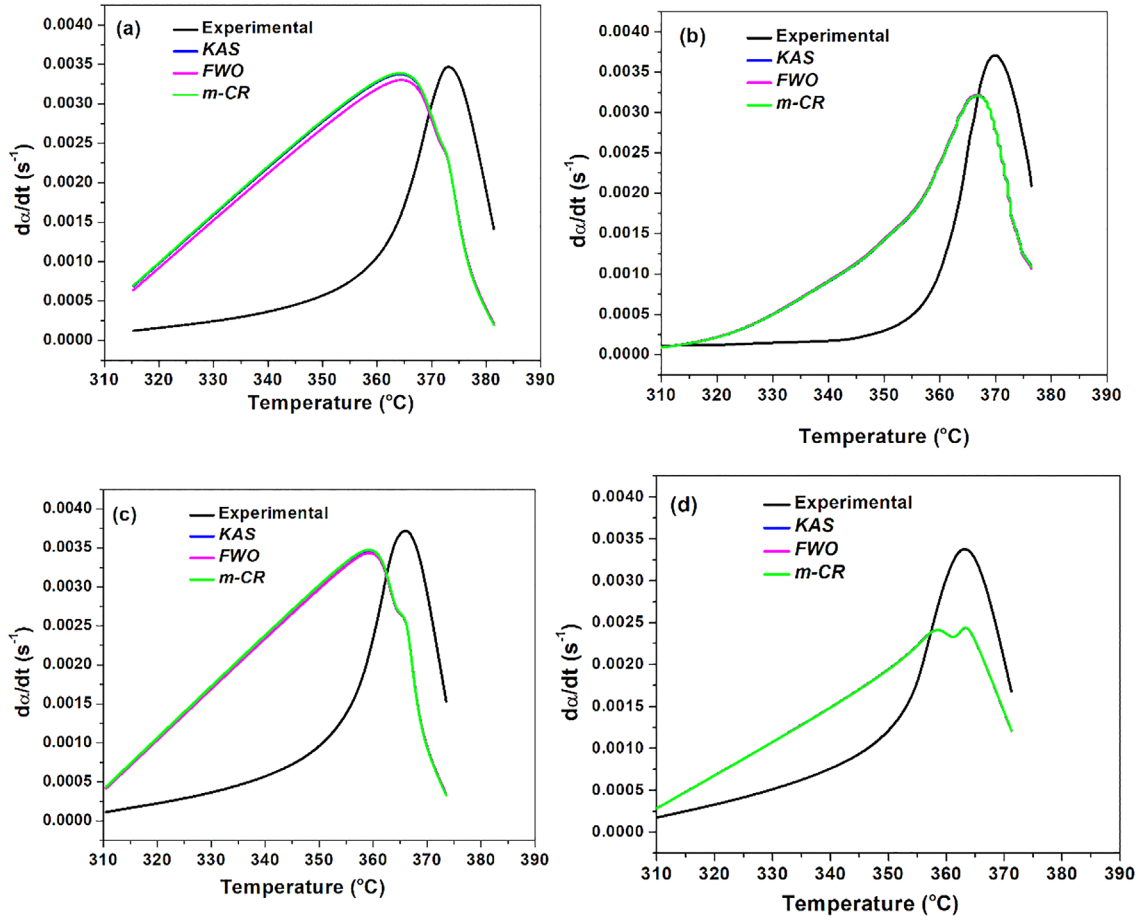

FIGURE 11 Predicted kinetics plots based on the nth order decomposition reaction model for blank PU and its nanocomposites containing various V-Al_2O_3 loadings at the heating rate of 5°C/min (a) blank PU; (b) PU/V-Al_2O_3-1; (c) PU/V-Al_2O_3-3; and (d)PU/V-Al_2O_3-5 [Color figure can be viewed at wileyonlinelibrary.com]

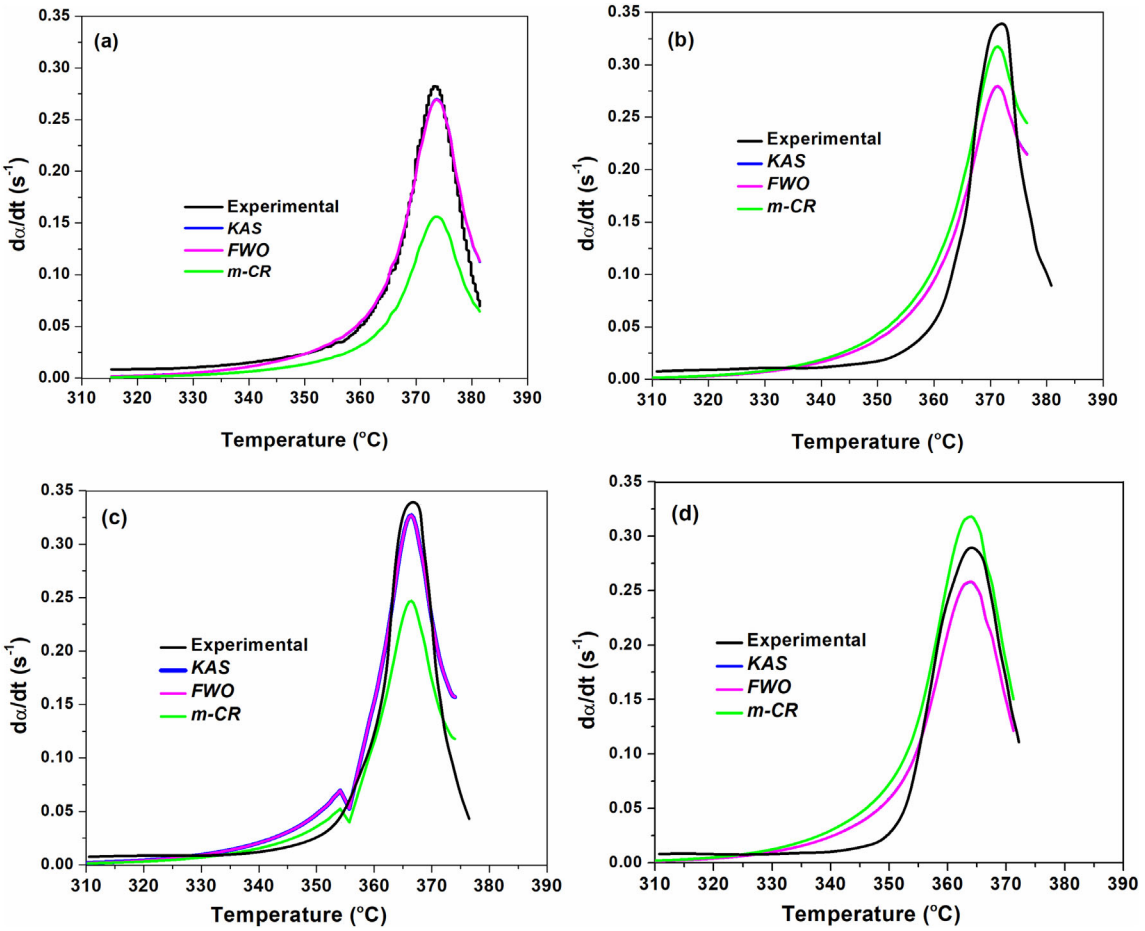

FIGURE 12 Predicted kinetics plots based on the Sestak and Berggren decomposition reaction model for blank PU and its nanocomposites containing various V-Al_2O_3 loadings at the heating rate of 5°C/min (a) blank PU; (b) PU/V-Al_2O_3-1; (c) PU/V-Al_2O_3-3; and (d) PU/V-Al_2O_3-5 [Color figure can be viewed at wileyonlinelibrary.com]

proved by increase in both E_α and ln(A). Figures 11 and 12 present the experimental and predicted values of the rate of decomposition reaction based on the nth order and Sestak and Berggren decomposition models respectively, for blank PU and its nanocomposites. As can be seen in Figure 11, the nth order model using integral methods showed more deviations from the experimental data. Furthermore, it is evident that the KAS, FWO, and m-CR equations have very similar sense of decomposition of samples. In contrast, as Figure 12 represents two kinetic exponents Sestak and Berggren equation shows a good correlation between the experimental and data fitted. Figure 12 suggests that there are more deviations from the experimental data as the V-Al_2O_3 loading increases.

4 | CONCLUSION

Nonisothermal decomposition kinetics of PU nanocomposites containing VTMS functionalized nano-Al_2O_3 particles was explored by varying the amount of V-Al_2O_3 loading. The increased T_5 of PU nanocomposite containing 1, 3, and 5 wt% of V-Al_2O_3 nanoparticles from 228.1 for PU to 268.7, 271.9, and 260.4°C for PU/V-Al_2O_3-1, PU/V-Al_2O_3-3, and PU/V-Al_2O_3-5 is attributed to the physical prevention effect of the V-Al_2O_3 nanoparticles which reduces escape of volatile compounds and free radicals produced through polymer chain-scission. Different integral isoconversional methods of FWO, KAS, and m-CR were used to estimate evolution of activation energy as a function of the partial mass loss. The average E_α values of PU nanocomposites varied from 157.62 for PU to 225.32, 183.07, and 229.19 (kJ/mol) for PU/V-Al_2O_3-1, PU/V-Al_2O_3-3, and PU/V-Al_2O_3-5, respectively. A rise in the E_α by introduction of V-Al_2O_3 nanoparticles in PU matrix indicated that polymer chains dissipate more energy and resist against thermal decomposition. It was found that the Sestak and Berggren model allows a more accurate description of the decomposition of PU and PU/V-Al_2O_3 nanocomposites compared to nth order model.

ORCID

Maryam Jouyandeh https://orcid.org/0000-0003-0435-6226

Henri Vahabi https://orcid.org/0000-0003-0419-7368

Mohammad Reza Saeb https://orcid.org/0000-0001-7860-5243

REFERENCES

[1] G. Gheno, R. Ganzerla, M. Bortoluzzi, R. Paganica, *Prog. Org. Coat.* **2015**, *78*, 239.

[2] D. Parra, L. P. Mercuri, J. Matos, H. F. Brito, R. Romano, *Thermochim. Acta* **2002**, *386*, 143.

[3] Z. Du, S. Wen, J. Wang, C. Yin, D. Yu, J. Luo, *J. Mater. Sci. Chem. Eng.* **2016**, *4*, 54.

[4] P. G. de Lange, *Powder coatings: Chemistry and technology*, Vincentz, Hanover, Germany **2004**.

[5] B. Utech, *A guide to high-performance powder coating*, Society of Manufacturing Engineers, Dearborn, MI **2002**.

[6] S. Papasavva, S. Kia, J. Claya, R. Gunther, *Prog. Org. Coat.* **2001**, *43*, 193.

[7] B. S. Hadavand, M. Ataeefard, H. F. Bafghi, *Compos. Part B Eng.* **2015**, *82*, 190.

[8] S. Rossi, M. Fedel, F. Deflorian, S. Zanol, *Mater. Des.* **2013**, *50*, 332.

[9] F. Xie, T. Zhang, P. Bryant, V. Kurusingal, J. M. Colwell, B. Laycock, *Prog. Polym. Sci.* **2019**, *90*, 211.

[10] S. Thomas, J. Datta, J. Haponiuk, A. Reghunadhan, *Polyurethane polymers: Blends and interpenetrating polymer networks*, Elsevier, Amsterdam **2017**.

[11] David, M. J.; Google Patents. **1953**.

[12] M. Bähr, A. Bitto, R. Mülhaupt, *Green Chem.* **2012**, *14*, 1447.

[13] B. Pilch-Pitera, *J. Appl. Polym. Sci.* **2010**, *116*, 3613.

[14] B. Pilch-Pitera, *J. Polym. Environ.* **2013**, *21*, 215.

[15] A. Madhi, B. Shirkavand Hadavand, A. Amoozadeh, *J. Compos. Mater.* **2018**, *52*, 2973.

[16] S. Rossi, M. Fedel, S. Petrolli, F. Deflorian, *J. Coat. Technol. Res.* **2016**, *13*, 427.

[17] A. Reghunadhan, M. Stranskowski, J. Datta, N. Kalarikkal, S. Thomas, *Macromol. Symp.* **2018**, *381*, 1800112.

[18] X. Liu, J. Hao, S. Gaan, *RSC Adv.* **2016**, *6*, 74742.

[19] M. Jouyandeh, S. M. R. Paran, M. Shabanian, S. Ghiyasi, H. Vahabi, M. Badawi, K. Formela, D. Puglia, M. R. Saeb, *Prog. Org. Coat.* **2018**, *123*, 10.

[20] M. Jouyandeh, M. Shabanian, M. Khaleghi, S. M. R. Paran, S. Ghiyasi, H. Vahabi, K. Formela, D. Puglia, M. R. Saeb, *Prog. Org. Coat.* **2018**, *125*, 384.

[21] H. Vahabi, M. Jouyandeh, M. Cochez, R. Khalili, C. Vagner, M. Ferriol, E. Movahedifar, B. Ramezanzadeh, M. Rostami, Z. Ranjbar, B. S. Hadavand, M. R. Saeb, *Prog. Org. Coat.* **2018**, *123*, 160.

[22] S. Ghiyasi, M. G. Sari, M. Shabanian, M. Hajibeygi, P. Zarrintaj, M. Rallini, L. Torre, D. Puglia, H. Vahabi, M. Jouyandeh, *Prog. Org. Coat.* **2018**, *120*, 100.

[23] M. Jouyandeh, O. M. Jazani, A. H. Navarchian, M. R. Saeb, *Color. Coat.* **2018**, *11*, 199.

[24] S. M. R. Paran, H. Vahabi, M. Jouyandeh, F. Ducos, K. Formela, M. R. Saeb, *J. Appl. Polym. Sci.* **2019**, *136*, 47483.

[25] M. Jouyandeh, E. Yarahmadi, K. Didehban, S. Ghiyasi, S. M. R. Paran, D. Puglia, J. A. Ali, A. Jannesari, M. R. Saeb, Z. Ranjbar, M. R. Ganjali, *Prog. Org. Coat.* **2019**, *123*, 10.

[26] S. Bayat, O. Moini Jazani, P. Molla-Abbasi, M. Jouyandeh, M. R. Saeb, *Prog. Org. Coat.* **2019**, *136*, 105201.

[27] Z. Karami, O. M. Jazani, A. H. Navarchian, M. Karrabi, H. Vahabi, M. R. Saeb, *Prog. Org. Coat.* **2019**, *129*, 357.

[28] Z. Karami, O. M. Jazani, A. H. Navarchian, M. R. Saeb, *Prog. Org. Coat.* **2018**, *125*, 222.

[29] V. T. Rathod, J. S. Kumar, A. Jain, *Appl. Nanosci.* **2017**, *7*, 519.

[30] Y. Wang, S. Lim, J. Luo, Z. Xu, *Wear* **2006**, *260*, 976.

[31] S. S. Golru, M. Attar, B. Ramezanzadeh, *Prog. Org. Coat.* **2014**, *77*, 1391.

[32] X. Chen, J. Yuan, J. Huang, K. Ren, Y. Liu, S. Lu, H. Li, *Appl. Surf. Sci.* **2014**, *311*, 864.

[33] M. Sangermano, M. Naguib, M. Messori, *Macromol. Mater. Eng.* **2013**, *298*, 1184.

[34] H.-J. Song, Z.-Z. Zhang, X.-H. Men, *Surf. Coat. Technol.* **2006**, *201*, 3767.

[35] A. Madhi, B. Shirkavand Hadavand, A. Amoozadeh, *Prog. Color Colorants Coat.* **2017**, *10*, 193.

[36] C. Sow, B. Riedl, P. Blanchet, *J. Coat. Technol. Res.* **2011**, *8*, 211.

[37] S. Siengchin, J. Karger-Kocsis, G. Psarras, R. Thomann, *J. Appl. Polym. Sci.* **2008**, *110*, 1613.

[38] H. Sui, X. Ju, X. Liu, K. Cheng, Y. Luo, F. Zhong, *Polym. Degrad. Stab.* **2014**, *101*, 109.

[39] F. Laoutid, L. Bonnaud, M. Alexandre, J.-M. Lopez-Cuesta, P. Dubois, *Mater. Sci. Eng. R: Rep.* **2009**, *63*, 100.

[40] X. Qian, L. Song, B. Yu, B. Wang, B. Yuan, Y. Shi, Y. Hu, R. K. Yuen, *J. Mater. Chem. A* **2013**, *1*, 6822.

[41] C. M. Becker, A. D. Gabbardo, F. Wypych, S. C. Amico, *Compos. A: Appl. Sci. Manuf.* **2011**, *42*, 196.

[42] K. Chrissafis, D. Bikiaris, *Thermochim. Acta* **2011**, *523*, 1.

[43] J. P. Jose, S. Thomas, *Phys. Chem. Chem. Phys.* **2014**, *16*, 14730.

[44] P. P. Lizymol, S. Thomas, *Polym. Degrad. Stab.* **1993**, *41*, 59.

[45] P. Das, P. Tiwari, *Thermochim. Acta* **2017**, *654*, 191.

[46] J. Xu, J. Sun, Y. Wang, J. Sheng, F. Wang, M. Sun, *Molecules* **2014**, *19*, 11465.

[47] M. F. Irfan, A. Arami-Niya, *Nano-Struct. Nano-Objects* **2019**, *18*, 100261.

[48] P. Salarizadeh, M. Javanbakht, S. Pourmahdian, A. Bagheri, H. Beydaghi, M. Enhessari, *J. Colloid Interface Sci.* **2016**, *472*, 135.

[49] M. Jouyandeh, N. Rahmati, E. Movahedifar, B. S. Hadavand, Z. Karami, M. Ghaffari, P. Taheri, E. Bakhshandeh, H. Vahabi, M. R. Ganjali, *Prog. Org. Coat.* **2019**, *133*, 220.

[50] M. Jouyandeh, O. M. Jazani, A. H. Navarchian, M. Shabanian, H. Vahabi, M. R. Saeb, *Appl. Surf. Sci.* **2018**, *447*, 152.

[51] H. Bockhorn, A. Hornung, U. Hornung, *J. Anal. Appl. Pyrolysis* **1999**, *50*, 77.

[52] F. Yao, Q. Wu, Y. Lei, W. Guo, Y. Xu, *Polym. Degrad. Stab.* **2008**, *93*, 90.

[53] M. R. Saeb, H. Rastin, M. Nonahal, S. M. R. Paran, H. A. Khonakdar, D. Puglia, *Prog. Org. Coat.* **2018**, *114*, 208.

[54] H. Rastin, M. R. Saeb, M. Nonahal, M. Shabanian, H. Vahabi, K. Formela, X. Gabrion, F. Seidi, P. Zarrintaj, M. G. Sari, P. Laheurte, *Prog. Org. Coat.* **2017**, *113*, 126.

[55] M. R. Saeb, H. Rastin, M. Shabanian, M. Ghaffari, G. Bahlakeh, *Prog. Org. Coat.* **2017**, *110*, 172.

[56] M. R. Saeb, M. Nonahal, H. Rastin, M. Shabanian, M. Ghaffari, G. Bahlakeh, S. Ghiyasi, H. A. Khonakdar, V. Goodarzi, *Prog. Org. Coat.* **2017**, *112*, 176.
[57] M. Nonahal, H. Rastin, M. R. Saeb, M. G. Sari, M. H. Moghadam, P. Zarrintaj, B. Ramezanzadeh, *Prog. Org. Coat.* **2018**, *114*, 233.
[58] N. Sbirrazzuoli, *Macromol. Chem. Phys.* **2007**, *208*, 1592.
[59] M. Ozawa, M. Kimura, A. Isogai, *J. Less Common Metals* **1990**, *162*, 297.
[60] H. E. Kissinger, *Anal. Chem.* **1957**, *29*, 1702.
[61] P. Kofstad, *Nature* **1957**, *179*, 1362.
[62] A. K. Burnham, R. L. Braun, *Energy Fuel* **1999**, *13*, 1.
[63] R. Ebrahimi-Kahrizsangi, M. Abbasi, *Trans. Nonferrous Metals Soc. China* **2008**, *18*, 217.
[64] D. W. van Krevelen, K. te Nijenhuis, *Properties of polymers: Their correlation with chemical structure; their numerical estimation and prediction from additive group contributions*, Elsevier, Amsterdam **2009**.
[65] V. Dhyani, J. Kumar, T. Bhaskar, *Bioresour. Technol.* **2017**, *245*, 1122.
[66] S. C. Turmanova, S. Genieva, A. Dimitrova, L. Vlaev, *Express Polym. Lett.* **2008**, *2*, 133.
[67] J. Šesták, G. Berggren, *Thermochim. Acta* **1971**, *3*, 1.
[68] P. K. Vimalathithan, C. Barile, C. Casavola, S. Arunachalam, M. G. Battisti, W. Friesenbichler, C. T. Vijayakumar, *Polym. Compos.* **2019**, *40*, 3634.

How to cite this article: Hadavand BS, Jouyandeh M, Paran SMR, et al. Silane-functionalized Al_2O_3-modified polyurethane powder coatings: Nonisothermal degradation kinetics and mechanistic insights. *J Appl Polym Sci*. 2020;e49412. https://doi.org/10.1002/app.49412